Inorganic Chemistry

Article

pubs.acs.org/IC

Prototypical Phosphine Complexes of Antimony(III)

Saurabh S. Chitnis,[†] Neil Burford,*[,†] Robert McDonald,[‡] and Michael J. Ferguson[‡]

[†]Department of Chemistry, University of Victoria, Victoria, British Columbia V8W 3V6, Canada

[‡]Department of Chemistry, University of Alberta, Edmonton, Alberta T6G 2G2, Canada

Supporting Information

ABSTRACT: Complexes of the generic formula $[Cl_n(PR_3)_mSb]^{(3-n)+}$ (n = 1, 2, 3, or 4 and m = 1 or 2) have been prepared featuring $[ClSb]^{2+}$, $[Cl_2Sb]^{1+}$, Cl_3Sb, or $[Cl_4Sb]^{1-}$ as acceptors with one or two phosphine ligands {PMe_3, PPh_3, PCy_3 (Cy = C_6H_{11})}. The solid-state structures of the complexes reveal foundational features that define the coordination chemistry of a lone pair bearing stibine acceptor site. The experimental observations are interpreted with dispersion-corrected density functional theory calculations to develop an understanding of the bonding and structural diversity.

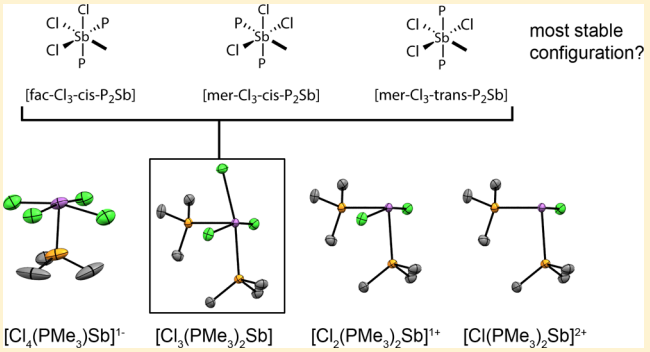

INTRODUCTION

The vast array of transition metal coordination complexes involving neutral two-electron donors is the foundation of classical coordination chemistry, which usually involves multiple ligands and is understood by invoking acceptor d-orbitals at the metal center. The donor−acceptor (Lewis acid−base) concept is extrapolated to describe adducts between p-block elements, referring to an acceptor with a single or multiple ligands [e.g., H_3NBH_3 and $(THF)_2AlH_3$, respectively]. For the relatively rare examples of electron-rich centers behaving as Lewis acceptors, the presence of a lone pair of electrons at the acceptor site[1] offers interesting structural and electronic features and some demonstrated applications in catalysis.[2] The most diverse array of complexes involving an electron-rich acceptor site is reported for monoantimony acceptors with phosphine ligands, including examples of neutral compounds,[3−5] anions,[6] and a broad array of cations. Stibenium cations can accommodate a single phosphine ligand to give the general structure **1**,[7−9] chelating diphosphine ligands to impose either structure **2** or **3**,[10] or two phosphine ligands in structural types **4**[8] and **5**.[10] In addition, two examples of the dication chelate complex structure **6**[10] and the unique tris-phosphine tricationic complex **7** have been reported.[11]

The structural diversity demonstrated by complexes of the type **1**−**7** prompted us to perform a systematic assessment of PR_3 complexes of chloro-antimony acceptors (R = Me, Ph, Cy). The potentially broad configurational variety for such compounds is illustrated in Chart 1 for the generic formula $[Cl_n(PR_3)_mSb]^{(3-n)+}$ (n = 2, 3, or 4 and m = 1 or 2) using an octahedral frame that includes a lone pair at the antimony acceptor site and in some cases a vacant coordination site. Our observations reveal substantial configurational versatility for antimony including examples of 9 of the 12 configurations listed in Chart 1. More importantly, the data provide for a rationalization of configurational preferences that define the coordination chemistry of a lone pair bearing stibine acceptor site, and this is confirmed by analogous observations for select derivatives of Cl_2PhSb and $[Ph_2Sb]^{1+}$ acceptors. The experimental observations are interpreted with dispersion-corrected density functonal theory (DFT) calculations to develop an understanding of the bonding and structural diversity. Together, the study debuts a coordination chemistry for antimony that has the potential to be as extensive and diverse as many transition metals.

EXPERIMENTAL SECTION

Reagents and Apparatus. All reagents were handled in a MBraun Labmaster 130 glovebox (dry N_2) or on a grease-free dual manifold argon and vacuum (base vacuum = 2×10^{-2} mbar) Schlenk line. Prior to use, HPLC-grade CH_3CN (Aldrich) was refluxed over CaH_2 for at least 48 h and distilled under an atmosphere of argon directly onto 3 Å molecular sieves, which had been freshly activated at 300 °C under dynamic vacuum for 24 h. All other solvents were obtained from an MBraun Solvent purification system and stored for at least 48 h over activated 4 Å molecular sieves prior to use. All reagents were purchased from Sigma-Aldrich. Deuterated solvents were dried using the same procedure as CH_3CN. $SbCl_3$ (99.99%) was purified by sublimation and $Sb(OTf)_3$ was prepared *in situ* from the metathesis of SbF_3 and $Me_3SiO_3SCF_3$ (TMSOTf). SbF_3 (99.99%), Ph_3P (97%), and Cy_3P (97%) were used as received. PMe_3 (97%) and TMSOTf (99%) were distilled before use. Reactions were carried out inside the glovebox in screw-cap glass vials that had been dried at 200 °C for at least 1 h and placed under dynamic vacuum (glovebox antechamber) while still hot. NMR tubes fitted with J-Young valves were charged and sealed inside the glovebox. Elemental analyses were carried out by Canadian Microanalytical Ltd. in Delta, British Columbia, Canada. All

Received: April 1, 2014
Published: April 28, 2014

   dx.doi.org/10.1021/ic500723y | *Inorg. Chem.* 2014, 53, 5359−5372

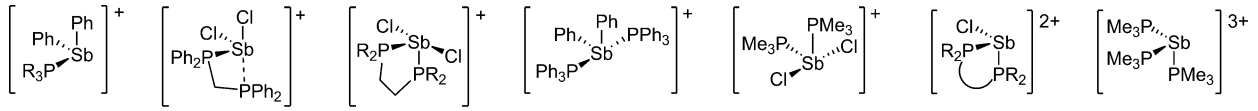

1 2 3 4 5 6 7

Chart 1. Potential Structural Variety (VSEPR-Inconsistent Structures Are Not Considered) in an Octahedral Frame for Antimony Complexes Composed of Four (Anion), Three (Neutral) or Two (Monocation) Chloride Substituents and One or Two Phosphine Ligands (P = PR_3)[a]

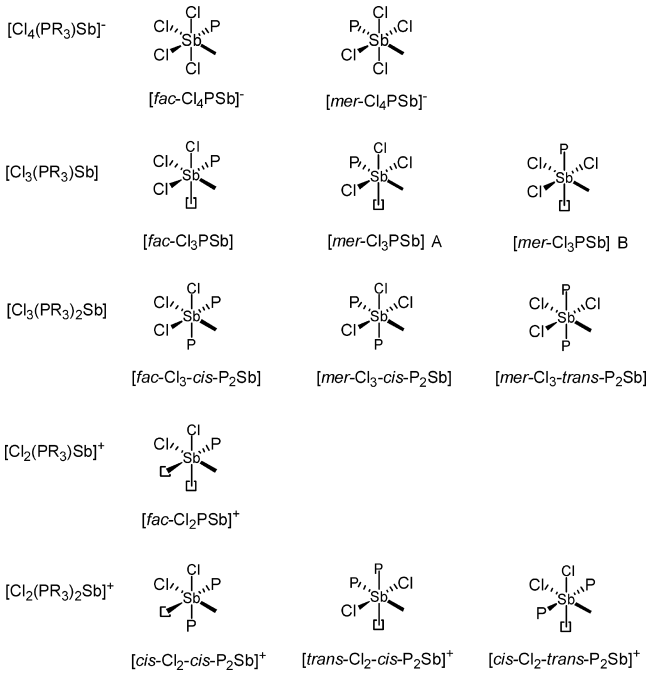

[a]The labels denote the abbreviated generic formula and distinguish between each configuration of the chloride substituents and the phosphine ligands. Bold line = lone pair; □ = vacant coordination site.

quantum chemical calculations were carried out using Gaussian 09. See Supporting Information for complete citation.

Preparation Procedures and Characterization Data. *[$Cl_3(PMe_3)Sb$].* PMe_3 (0.08 g, 1.0 mmol) and $SbCl_3$ (0.23 g, 1.0 mmol) were combined in CH_3CN. The resulting white suspension was stirred for 1 h and then allowed to settle. Crystals were obtained from the supernatant by slow evaporation. Yield: 0.27 g, 88%. Elemental analysis for $C_3H_9Cl_3PSb$ (calcd./expt.): C (11.85/11.87), H (2.98/3.22). Melting point: 188−190 °C. NMR (CD_3CN, 298 K, 7.05 T field strength): ^1H: 1.98 ppm (*d*, $^2J_{H-P}$ = 14.3 Hz), $^{13}C\{^1H\}$: 10.1 ppm, (*d*, $^1J_{C-P}$ = 35 Hz), $^{31}P\{^1H\}$: 9.6 ppm (*s*).

[$Cl_3(PPh_3)Sb$]. $SbCl_3$ (0.23 g, 1.0 mmol) and PPh_3 (0.26 g, 1.0 mmol) were combined in CH_2Cl_2 (4 mL) to obtain a clear, golden yellow solution, which was stirred for 1 h. The reaction mixture was filtered and concentrated under a vacuum to ca. 2 mL and stored at room temperature for 24 h, which led to the formation of small yellow crystals. The reaction mixture was removed from vacuum and allowed to sit at room temperature for 24 h, which led to the formation of yellow block-shaped crystals that were washed with 0.5 mL of cold CH_2Cl_2 and dried under a vacuum. Yield: 0.41 g, 84%. Melting point: 120−122 °C. Elemental analysis for $C_{18}H_{15}Cl_3PSb$ (calcd/expt): C (44.09/44.97), H (3.08/3.23). NMR (CD_2Cl_2, 298 K, 7.0 T field strength): ^1H: 7.1−7.9 (*m*, Ph_3P), $^{13}C\{^1H\}$: 128.4 ppm (*d*, $^1J_{C-P}$ = 25.0 Hz), $^{31}P\{^1H\}$: 5.6 ppm (*s*).

[$Cl_3(PCy_3)Sb$]. $SbCl_3$ (0.11 g, 0.50 mmol) and PCy_3 (0.14 g, 0.50 mmol) were combined in 3 mL of CH_2Cl_2 to obtain a light yellow solution. The reaction mixture was stirred for 20 min, filtered through glass wool, and concentrated under a vacuum to 1 mL. Very pale yellow block-like crystals were obtained over 48 h at −30 °C, isolated by decantation, washed with 0.5 mL of cold CH_2Cl_2 and dried under a vacuum. Yield: 0.21 g, 82%. Melting point: 142−145 °C (dec). Elemental analysis for $C_{18}H_{33}Cl_3SbP$ (calcd/expt): C (42.51/42.73), H (6.54/6.63). NMR (CD_2Cl_2, 298 K, 8.45 T field strength): ^1H: 1.36−1.92 ppm (*m*, 10*H*), 3.23 ppm (*tq*, 12.9 Hz, 2.6 Hz, 1*H*), $^{13}C\{^1H\}$: 26.3 ppm, (s), 27.82 (*d*, $^3J_{C-P}$ = 11.2 Hz), 29.65 (*d*, $^2J_{C-P}$ = 4.8 Hz), 33.85 (*d*, $^1J_{C-P}$ = 15.0 Hz), $^{31}P\{^1H\}$: 25.1 ppm (*s*).

[$Cl_3(PMe_3)_2Sb$]. A solution of PMe_3 (0.46 g, 6.0 mmol) in 4 mL of CH_3CN was added to $SbCl_3$ (0.68 g, 3.0 mmol) dissolved in 4 mL of CH_3CN. Midway through the addition a large amount of white precipitate appeared. By the end of the addition a clear, pale yellow solution was obtained which was allowed to stir for 30 min, concentrated under a vacuum to ca. 2 mL and filtered through glass wool. Colorless blocks were obtained by diffusion of Et_2O into the concentrated CH_3CN solution. The crystals were washed with cold CH_3CN and dried under a vacuum. Yield: 1.10 g, 97%. Melting point: 110−113 °C (dec). Elemental analysis for $C_6H_{18}C_{l3}SbP_2$ (calcd/expt): C (18.95/18.84), H (4.77/4.59). NMR (CD_3CN, 298 K, 8.45 T field strength): ^1H: 1.76 ppm (*d*, $^2J_{H-P}$ = 11.33 Hz), $^{13}C\{^1H\}$: 11.9 ppm (*d*, $^1J_{C-P}$ = 25.0 Hz), ^{31}P: −10.2 ppm (*m*, $^2J_{P-H}$ = 11.2 Hz).

[$Cl_3(PPh_3)_2Sb$]. PPh_3 (0.52 g, 2.0 mmol) and $SbCl_3$ (0.23 g, 1.0 mmol) were combined in 5 mL of CH_2Cl_2. The resulting clear yellow solution was stirred for 1 h, filtered through glass wool, concentrated under a vacuum to 2 mL, and recrystallized at −30 °C to obtain light yellow translucent crystals. The crystals were isolated by decantation, washed with 0.5 mL of cold CH_2Cl_2, and dried under a vacuum. Yield: 0.65 g 86%. Melting point: 115−118 °C. Elemental analysis for $C_{36}H_{30}Cl_3SbP_2$ (calcd/expt): C (57.45/57.75), H (4.02/4.39). NMR (CD_2Cl_2, 298 K, 7.0 T field strength): ^1H: 7.1−7.9 (*m*, PPh_3), $^{13}C\{^1H\}$: 128.4 ppm (*d*, $^1J_{C-P}$ = 25.0 Hz), $^{31}P\{^1H\}$: 5.6 ppm (*s*).

[$Cl_3(PCy_3)_2Sb$]. $SbCl_3$ (0.11 g, 0.50 mmol) and PCy_3 (0.28 g, 1.0 mmol) were combined in a 3 mL of CH_3CN. The reaction mixture was stirred for 16 h to get a light yellow suspension. The supernatant was removed, and the precipitate was washed with 3 mL of cold CH_3CN and pumped dry. The supernatant was concentrated under a vacuum to obtain yellow needle-shaped crystals. The crystals and bulk powder exhibited identical NMR spectra, although trace amounts of $[Cl_3(PCy_3)Sb]$ was also found in the bulk and could not be separated by recrystallization. Yield (impure): 0.66 g. Melting point: 135−138 °C. Elemental analysis for $C_{36}H_{66}Cl_3P_2Sb$ (calcd/expt): C (54.80/52.38), H (8.43/8.07). NMR (CD_2Cl_2, 298 K, 7.0 T field strength): ^1H: 1.34−2.56 ppm (*m*), $^{31}P\{^1H\}$: 15.7 ppm (*s*).

[$Cl_2(PMe_3)Sb$][OTf]. $SbCl_3$ (0.11 g, 0.50 mmol) and TMSOTf (0.11 g, 0.50 mmol) were combined in 2.5 mL of CH_3CN and stirred for 1 h. A solution of PMe_3 (0.04 g, 0.50 mmol) in 2 mL of CH_3CN was added, and the reaction mixtures were stirred for 1 h to obtain a clear, colorless solution. All volatiles were removed under a vacuum to obtain a white powder (0.207 g, calcd. for product 0.209 g), which was recrystallized from CH_3CN at −30 °C to obtain colorless block-shaped crystals, which were washed with cold CH_3CN and dried under a vacuum. Yield: 0.19 g, 91%. Melting point: 108−111 °C. Elemental analysis for $C_4H_9Cl_2F_3O_3PSSb$ (calcd/expt): C (11.49/11.37), H (2.17/2.19). NMR (CD_3CN, 298 K, 8.45 T field strength): ^1H: 1.99 ppm (*d*, $^2J_{H-P}$ = 14.7 Hz), $^{13}C\{^1H\}$: 9.7 ppm (*d*, $^1J_{C-P}$ = 34.1 Hz), $^{31}P\{^1H\}$: 14.6 ppm (*s*), $^{19}F\{^1H\}$: −80.0 ppm (*s*).

[$Ph_2(PMe_3)Sb$][OTf]. $Sb(OTf)_3$ (0.29 g, 0.50 mmol) and $SbPh_3$ (0.35 g, 1.0 mmol) were combined in CH_3CN (4 mL) and stirred for 1 h to get a pale yellow solution of Ph_2SbOTf. Neat PMe_3 (0.11 g, 1.5 mmol) was added in three portions to obtain a clear, light yellow solution. This reaction mixture was stirred for 40 min, filtered through glass wool, concentrated under a vacuum to approximately 2 mL.

dx.doi.org/10.1021/ic500723y | Inorg. Chem. 2014, 53, 5359−5372

Table 1. Crystal Data for the Featured Compounds

	$[Cl_3(PMe_3)Sb]$	$[Cl_3(PPh_3)Sb]$	$[Cl_3(PCy_3)Sb]$	$[Cl_3(PMe_3)_2Sb]$	$[Cl_3(PPh_3)_2Sb]$	$[Cl_3(PCy_3)_2Sb]$
formula	$C_3H_9Cl_3PSb$	$C_{18}H_{15}Cl_3PSb$	$C_{18}H_{33}Cl_3PSb$	$C_6H_{18}Cl_3P_2Sb$	$C_{36}H_{30}Cl_3P_2Sb$	$C_{36}H_{66}Cl_3P_2Sb$
fw	304.17	490.37	508.51	380.24	752.64	788.93
space grp	$P2_1/n$	$P\bar{1}$	$P\bar{1}$	$P2_1/n$	$I2/a$	$P\bar{1}$
a /Å	7.9261 (11)	10.5374 (8)	10.376 (3)	7.6594 (4)	15.8017 (12)	9.7577 (7)
b /Å	19.089 (3)	10.5630 (8)	15.895 (4)	11.4178 (6)	9.5425 (8)	10.3383 (7)
c /Å	13.1115 (18)	10.6579 (8)	20.641 (5)	16.0941 (8)	22.4802 (18)	11.2342 (8)
α /deg		92.9183 (8)	85.320 (4)			115.1065 (7)
β/ deg	100.8495 (17)	115.7836 (7)	80.800 (4)	96.3001 (5)	101.4987 (9)	104.6530 (7)
γ /deg		113.9875 (7)	73.177 (4)			94.0515 (8)
V /Å^3	1948.3 (5)	937.79 (12)	3214.2 (14)	1398.98 (12)	3321.7 (5)	972.13 (12)
Z	8	2	6	4	4	1
ρ /g cm^{-3}	2.074	1.737	1.576	1.805	1.505	1.348
λ /Å	0.710 73	0.710 73	0.710 73	0.710 73	0.710 73	0.710 73
T /K	173	173	173	173	173	173
GOF	1.036	1.102	0.872	1.048	1.068	1.079
R_1	0.0259	0.0190	0.0394	0.0123	0.0204	0.0250
wR_2	0.0513	0.0455	0.0776	0.0295	0.0507	0.0672

	$[Cl_2(PMe_3)Sb][OTf]$	$[Ph_2(PMe_3)Sb][OTf]$	$[Cl_2(PPh_3)_2Sb][OTf]$	$[Ph_2(PMe_3)_2Sb][OTf]$	$[Cl(PMe_3)_2Sb][OTf]_2$	$[Mg(CH_3CN)_6][Cl_4(PMe_3)Sb]_2$
formula	$C_4H_9Cl_2F_3O_3PSSb$	$C_{16}H_{19}F_3O_3PSSb$	$C_{37}H_{30}Cl_2F_3O_3P_2SSb$	$C_{19}H_{28}F_3O_3P_2SSb$	$C_8H_{18}ClF_6O_6P_2S_2Sb$	$C_{18}H_{36}Cl_8MgN_6P_2Sb_2$
fw	417.79	501.09	866.26	577.16	607.48	949.88
space grp	$P2_1/c$	$P\bar{1}$	$P\bar{1}$	$P2_1/c$	$P2_1/n$	$P2_12_12_1$
a /Å	10.798 (2)	8.2553 (2)	9.5641 (7)	8.2974 (3)	13.5151 (8)	10.9776 (15)
b /Å	11.059 (2)	10.8326 (3)	12.0248 (8)	11.1805 (4)	11.4915 (7)	10.9983 (15)
c /Å	12.214 (3)	11.1367 (3)	17.5876 (12)	26.4962 (9)	13.9937 (8)	32.060 (4)
α /deg		98.4361 (3)	94.0493 (9)			
β/ deg	114.382 (2)	97.6027 (3)	96.8668 (10)	93.3876 (4)	105.7092 (6)	
γ /deg		93.1231 (3)	110.3615 (9)			
V /Å^3	1328.5 (5)	973.70 (4)	1869.0 (2)	2453.73 (15)	2092.2 (2)	3870.7 (9)
Z	4	2	2	4	4	4
ρ /g cm^{-3}	2.089	1.709	1.539	1.562	1.929	1.630
λ /Å	0.710 73	0.710 73	0.710 73	0.710 73	0.710 73	0.710 73
T /K	173	173	173	173	173	173
GOF	1.081	1.063	1.062	1.050	1.037	1.063
R_1	0.0313	0.0157	0.0289	0.0201	0.0175	0.0367
wR_2	0.0810	0.0413	0.0719	0.0506	0.0434	0.0797

	$[Cl_2(Ph)(PMe_3)Sb]$	$[Cl_2(Ph)(PPh_3)Sb]$	$[Cl_2(Ph)(PPh_3)_2Sb]$
formula	$C_9H_{14}Cl_2PSb$	$C_{24}H_{20}Cl_2PSb$	$C_{42}H_{35}Cl_2P_2Sb$
fw	345.82	532.02	794.29
space grp	$P2_1/n$	$P2_1/n$	$C2/c$
a /Å	6.8302 (2)	10.3232 (4)	12.9097 (2)
b /Å	17.8515 (5)	11.6723 (4)	14.2568 (2)
c /Å	10.5339 (3)	18.4318 (7)	19.9245 (3)
α /deg			
β/ deg	93.8302 (3)	90.4966 (4)	96.6050 (7)
γ/ deg			
V /Å^3	1281.52 (6)	2220.87 (14)	3642.78 (9)
Z	4	4	4
ρ /g cm^{-3}	1.792	1.591	1.448
λ /Å	0.710 73	0.710 73	0.710 73
T /K	173	173	173
GOF	1.173	1.149	1.111
R_1	0.0163	0.0230	0.0185
wR_2	0.0411	0.0555	0.0474

Colorless crystals were obtained upon storage −30 °C for 24 h, isolated by removing the supernatant by pipet and washed with 0.5 mL of cold CH_3CN and dried under a vacuum. Yield: 0.42 g, 83%. Melting point: 117−119 °C. Elemental analysis for $C_{16}H_{19}F_3O_3PSSb$ (calcd/expt): C (38.35/38.66) H (3.82/3.88). NMR (CD_3CN, 298 K, 7.05 T field strength): ^{1}H: 1.60 ppm (*d*, $^2J_{H-P}$ = 13.5 Hz, 9*H*), 7.52−7.57 ppm (*m*, 6*H*), 7.67−7.72 (*m*, 4*H*), ^{13}C{^{1}H}: 10.3 ppm (*d*, $^1J_{C-P}$ = 31.9 Hz), 130.9 ppm (*s*), 131.6 ppm (*s*), 138.1 ppm (*s*), ^{31}P{^{1}H}: −21.2 ppm (*s*), ^{19}F: ppm (*s*): −79.2 ppm (*s*).

[$Cl_2(PMe_3)_2Sb$][OTf]. $SbCl_3$ (0.23 g, 1.0 mmol) and TMSOTf (0.22 g, 1.0 mmol) were combined in CH_2Cl_2 (4 mL) and stirred for 30 min to yield a clear and colorless solution. This was added dropwise to a

dx.doi.org/10.1021/ic500723y | Inorg. Chem. 2014, 53, 5359−5372

Scheme 1. Synthetic Approaches to Prototypical Complexes of Antimony(III)

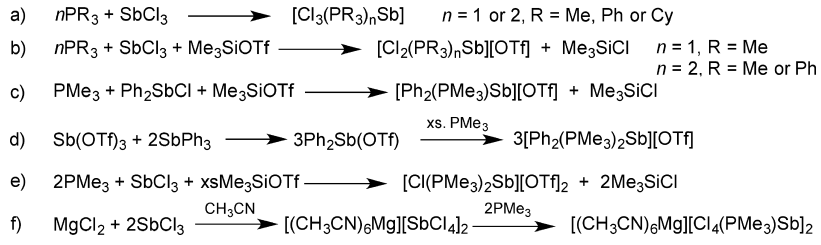

stirring solution of PMe_3 (0.228 g, 3.00 mmol) in CH_2Cl_2 (4 mL) over 30 s to produce a cloudy white suspension. The reaction mixture was allowed to stir for 1 h yielding a fine white powder and a clear and colorless supernatant, the $^{31}P\{^1H\}$ NMR spectrum of which exhibited two signals (5.8 ppm, 85% and −2.2 ppm, 15%). Removal of solvent under dynamic vacuum at room temperature over 4 h yielded a fine white powder (0.515 g), which was recrystallized in CH_3CN (10 mL) at −30 °C. Highly reflective colorless block-shaped crystals were obtained after 5 days, isolated by decantation, washed with cold CH_3CN (3 × 3 mL); Yield: 0.40 g, 80%; melting point: 135 °C dec.; elemental analysis calcd (found): C 17.02 (16.97), H 3.67 (3.41); NMR: ^1H (CD_3CN, 500 MHz, 293 K): 2.08 (*d*, 18H, $^2J_{PH}$ = 14.1 Hz); $^{13}C\{^1H\}$ NMR (CD_3CN, 125.76 MHz, 293 K): 11.6 (*d*, $^1J_{PC}$ = 34.4 Hz), 118.5 (*s*); ^{19}F NMR (CD_3CN, 282.44 MHz, 293 K): −79.1 (*s*); $^{31}P\{^1H\}$ NMR (CD_3CN, 202.46 MHz, 293 K): 6.2 (*s*).

[$Cl_2(PPh_3)_2Sb$][OTf]. To a solution of $SbCl_3$ (0.09 g, 0.40 mmol) in CH_2Cl_2 (1 mL) was added a solution of PPh_3 (0.11 g, 0.40 mmol) in CH_2Cl_2 (1 mL). Neat TMSOTf (0.09 g, 0.40 mmol) was added, and the clear, bright yellow solution was stirred at room temperature. Following filtration through glass wool and concentration under reduced vacuum, crystalline yellow blocks were obtained after storage at room temperature for 24 h. The crystals were washed with 0.5 mL of cold CH_2Cl_2 and dried under a vacuum. Yield: 0.66 g, 76%. Melting point: 105 °C (dec.). Elemental analysis for $C_{37}H_{30}Cl_2F_3O_3P_2SSb$ (calcd/expt): C (51.30/51.05), H (3.49/3.01). NMR (298 K, 11.7 T field strength): ^1H ($CDCl_3$): 7.46−7.57 ppm (*m*, Ph), $^{13}C\{^1H\}$ ($CDCl_3$): 128.4 (*d*, $^1J_{C-P}$ = 24 Hz), 129.2 (*d*, $^3J_{C-P}$ = 10 Hz), 131.3 (*s*), 134.0 (*d*, $^2J_{C-P}$ = 13 Hz), $^{31}P\{^1H\}$(CD_2Cl_2): −5.0 ppm (*s*, broad).

[$Ph_2(PMe_3)_2Sb$][OTf]. A solution of $Sb(OTf)_3$ (0.29 g, 0.50 mmol) and $SbPh_3$ (0.35 g, 1.0 mmol) were combined in CH_3CN (4 mL) and stirred for 1 h to get a pale yellow solution. All volatiles were removed under a vacuum to yield an off-white powder, which was not isolated. The powder was redissolved in CH_2Cl_2 (3 mL), and a solution of PMe_3 (0.34 g, 4.5 mmol) in CH_2Cl_2 (3 mL) was dropwise added to get a clear, very light brown solution. This reaction mixture was stirred for 10 min, filtered, concentrated under a vacuum to approximately 3 mL. Large, colorless blocks, obtained upon recrystallization at −30 °C over 24 h, were isolated by removing the supernatant by pipet and were washed with 0.5 mL cold CH_2Cl_2 and dried under a vacuum. Yield: 0.69 g, 80%. Melting point: 98−100 °C. Elemental analysis for $C_{19}H_{29}F_3O_3P_2SSb$ (calcd/expt): C (39.54/39.96), H (4.89/4.68). NMR (CD_2Cl_2, 298 K, 8.45 T field strength): ^1H: 1.19 ppm (*d*, $^2J_{H-P}$ = 7.9 Hz, 18*H*), 7.53−7.59 ppm (*m*, 6*H*), 7.65−7.69 (*m*, 4*H*), $^{13}C\{^1H\}$: 12.2 ppm (*d*, $^1J_{C-P}$ = 12.1 Hz), 130.6 ppm (*s*), 131.0 ppm (*s*), 136.6 ppm (*s*), $^{31}P\{^1H\}$: −41.3 ppm (*s*), ^{19}F: −79.2 ppm (*s*).

[$Cl(PMe_3)_2Sb$][OTf]$_2$. A solution of excess TMSOTf (0.67 g, 3.0 mmol) in 4 mL of CH_3CN was added to solid [$(PMe_3)_2Cl_3Sb$] (0.38 g, 1.0 mmol), and the clear, colorless solution was allowed to stir for 1 h. Volatiles were removed under a vacuum to yield a sticky powder, which was redissolved in a minimum of CH_3CN and recrystallized via diffusion of Et_2O at −30 °C to give colorless block-shaped crystals that were washed with 0.5 mL of cold CH_3CN. Yield: 0.50 g, 82%. Melting point: 157−160 °C. Elemental analysis for $C_8H_{18}ClF_6O_6P_2S_2Sb$ (calcd/expt): C (15.81/15.45), H (2.99/2.83). NMR (CD_3CN, 298 K, 8.45 T field strength): ^1H: 2.0 ppm (d, $^2J_{H-P}$ = 14.6 Hz), $^{13}C\{^1H\}$: 9.6 ppm (*d*, $^1J_{C-P}$ = 34.0 Hz), $^{31}P\{^1H\}$: 15.8 (*s*, broad).

[$Mg(CH_3CN)_6$][$Cl_4(PMe_3)Sb$]$_2$. $MgCl_2$ (0.10 g, 1.0 mmol) and $SbCl_3$ (0.46 g, 2.0 mmol) were combined in 8 mL of CH_3CN. The reaction mixture was stirred for 16 h to obtain a white suspension. Neat PMe_3 (0.16 g, 2.0 mmol) was added to obtain a clear solution, which became cloudy upon stirring for an additional 1 h. The supernatant was removed from the white precipitate and filtered. Slow removal of CH_3CN at room temperature yielded colorless crystalline blocks. The dried precipitate and crystals gave identical ^{31}P, ^1H, and ^{13}C NMR spectra. Yield: 0.78 g, 74%. Melting point: 175−178 °C (dec). Samples prepared for elemental analysis (dynamic vacuum for 24 h) show loss of one molecule of CH_3CN giving [$Mg(CH_3CN)_5$][$Cl_4(PMe_3)Sb$]$_2$, $C_{16}H_{33}N_5Sb_2MgCl_8P$ (calcd/expt): C (21.14/21.27), H (3.66/3.49), N(7.71/7.84). NMR (CD_3CN, 298 K, 8.45 T field strength): ^1H: 1.95 ppm (*d*, 18H, $^2J_{H-P}$ = 14.2 Hz, PMe_3); 1.99 ppm (*s*, 18H, CH_3CN), $^{13}C\{^1H\}$: 10.4 ppm (*d*, $^1J_{C-P}$ = 36.2 Hz), $^{31}P\{^1H\}$: 7.7 ppm (*s*, broad).

[$Cl_2(Ph)(PMe_3)Sb$]. A solution of PMe_3 (0.04 g, 0.50 mmol) in 1 mL of CH_3CN was added to $PhSbCl_2$ (0.13 g, 0.50 mmol) dissolved in 3 mL of CH_3CN. The clear colorless reaction mixture was allowed to stir for 15 min, filtered, and concentrated under a vacuum at room temperature to obtain clear colorless crystalline blocks that were washed with 0.5 mL of cold CH_3CN and dried under a vacuum. Yield: 0.30 g, 86%. Melting point: 147−149 °C. Elemental analysis for $C_9H_{14}Cl_2PSb$ (calcd/expt): C (31.26/31.53), H (4.08/4.19). NMR (CD_3CN, 298 K, 7.05 T field strength): ^1H: 1.75 ppm (*d*, $^2J_{H-P}$ = 13.9 Hz, 9*H*), 7.38−7.52 ppm (*m*, 3*H*), 8.29 ppm (*m*, 2*H*), $^{13}C\{^1H\}$: 10.2 ppm, (*d*, $^1J_{C-P}$ = 35 Hz), $^{31}P\{^1H\}$: −9.2 ppm (*s*).

[$Cl_2(Ph)(PPh_3)Sb$]. A solution of PPh_3 (0.262 g, 1 mmol) in 2 mL of CH_2Cl_2 was added to $PhSbCl_2$ (0.260 g, 1 mmol) dissolved in 2 mL of DCM. The clear golden yellow reaction mixture was allowed to stir for 15 min, filtered, and concentrated under vacuum to ca. 1 mL. Yellow crystalline blocks were obtained by diffusion of pentane vapor into this solution at −30 °C over 24 h and isolated by decanting the supernatant. Yield: 0. 217 g, 42%. Melting point: 118 °C dec; NMR (CD_2Cl_2, 298 K, 8.45 T field strength): ^1H: 7.1−7.9 (*m*, Ph_3P), $^{13}C\{^1H\}$: 128.4 ppm (*d*, $^1J_{C-P}$ = 25.0 Hz), $^{31}P\{^1H\}$: 5.6 ppm (*s*) .

Structure Determination of [$Cl_2(Ph)(PPh_3)_2Sb$]. This product could not be isolated as a pure substance and was formed together with [$Cl_2(Ph)(PPh_3)Sb$]. A solution of PPh_3 (0.262 g, 1 mmol) in 2 mL of CH_3CN was added to $PhSbCl_2$ (0.130 g, 1 mmol) to obtain a yellow solution, which was allowed to stir for 40 min. Upon concentration to 1 mL at −30 °C for 72 h, a mixture of yellow and colorless crystals was obtained, and the colorless crystals were identified as [$Cl_2(Ph)$-(PPh_3)$_2$Sb] by X-ray crystallography. It was not possible to manually isolate a sufficient quantity of the colorless crystals to characterize the compound as a pure substance.

RESULTS AND DISCUSSION

Preparation of Phosphine Complexes of Antimony. A series of PR_3 (R = Me, Ph, Cy) complexes on $[ClSb]^{2+}$, $[Cl_2Sb]^{1+}$, Cl_3Sb, or $[Cl_4Sb]^{1-}$ acceptors have been prepared and structurally characterized. As illustrated in Scheme 1a, reactions of PR_3 with $SbCl_3$ yield the corresponding derivatives of [$Cl_3(PR_3)Sb$]. In the presence of excess phosphine the bis-phosphine complexes, [$Cl_3(PR_3)_2Sb$], are formed. Analogous reactions of $Cl_2(Ph)Sb$ with PR_3 give the corresponding derivatives of [$Cl_2(Ph)(PR_3)Sb$]. Attempts to prepare [$Cl_2(Ph)(PMe_3)_2Sb$] yielded only [$Cl_2(Ph)(PMe_3)Sb$] and free PMe_3 even in the presence of a 6-fold excess of phosphine.

dx.doi.org/10.1021/ic500723y | Inorg. Chem. 2014, 53, 5359−5372

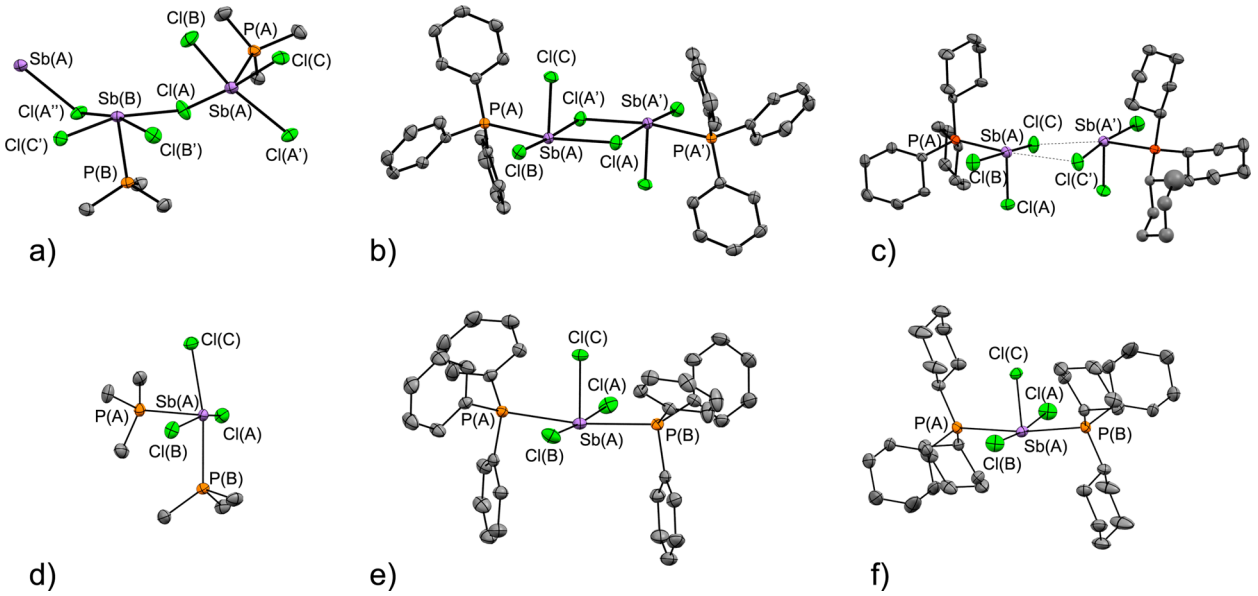

Figure 1. Views of the solid-state structures for (a) [*mer*-$Cl_3(PMe_3)Sb$] (showing Sb−Cl intermolecular interactions that results in a polymeric array), (b) [*fac*-$Cl_3(PPh_3)Sb$] (dimeric structure), (c) [*mer*-$Cl_3(PCy_3)Sb$], (d) [*mer*-Cl_3-*cis*-$(PMe_3)_2Sb$], (e) [*mer*-Cl_3-*trans*-$(PPh_3)_2Sb$], and (f) [*mer*-Cl_3-*trans*-$(PCy_3)_2Sb$].

We speculate that the Lewis acidity of the antimony center in $[Cl_2(Ph)(PR_3)Sb]$ is quenched by PMe_3, but not by PPh_3.

Reaction of PMe_3 with $SbCl_3$ in the presence of 1 equivalent of TMSOTf gives $[Cl_2(PMe_3)Sb][OTf]$ with elimination of TMSCl as illustrated in Scheme 1b, while attempts to obtain $[Cl_2(PPh_3)Sb][OTf]$ were unsuccessful, giving only $[Cl_2(PPh_3)_2Sb][OTf]$. The corresponding $[Cl_2(PMe_3)_2Sb][OTf]$ is formed in the presence of 2 equivalents or excess PMe_3. The analogous reaction of PMe_3 with Ph_2SbCl and TMSOTf gives $[Ph_2(PMe_3)Sb][OTf]$ according to Scheme 1c, and $[Ph_2(PMe_3)_2Sb][OTf]$ is formed according to Scheme 1d from $Ph_2(OTf)Sb$ [generated *in situ* via substituent exchange between $(OTf)_3Sb$ and Ph_3Sb].

In the presence of excess TMSOTf, mixtures of PMe_3 with $SbCl_3$ yield $[Cl(PMe_3)_2Sb][OTf]_2$, as in Scheme 1e. Attempts to prepare the PPh_3 derivative were unsuccessful, resulting in formation of $[Cl_2(PPh_3)_2Sb][OTf]$ even in the presence of a large excess of TMSOTf. Reaction of PMe_3 with $MgCl_2$ and $SbCl_3$ in CH_3CN yields $[Mg(CH_3CN)_6][Cl_4(PMe_3)Sb]_2$, according to Scheme 1f. However, there is no evidence of an analogous reaction occurring with PPh_3.

Structure and Bonding in Neutral Phosphine Complexes of Antimony. The structural features of the neutral complexes $[Cl_3(PMe_3)Sb]$, $[Cl_3(PPh_3)Sb]$, $[Cl_3(PCy_3)Sb]$, $[Cl_3(PMe_3)_2Sb]$, $[Cl_3(PPh_3)_2Sb]$, and $[Cl_3(PCy_3)_2Sb]$ are illustrated in Figure 1, and selected structural parameters are listed in Table 2. In the solid state, $[Cl_3(PMe_3)Sb]$ adopts a polymeric arrangement in which antimony centers are bridged by chlorine centers that impose a distorted square planar $SbCl_4$ frame with a phosphine center in an axial position. The Sb−Cl distances involving the bridging chlorine centers are predictably longer than those involving the terminal chlorine centers. Considering the shortest Sb−Cl interactions (Figure 2), we envisage a lone pair of electrons occupying the site *trans* to the phosphine ligand in the square-based pyramid, representing the configuration [*mer*-Cl_3PSb] A, illustrated in Chart 1.

Dimeric arrangements are observed for $[Cl_3(PPh_3)Sb]$ and $[Cl_3(PCy_3)Sb]$ in the solid state, which represent configurations [*fac*-Cl_3PSb] and [*mer*-Cl_3PSb] B, respectively (Chart 1). In each case, two chlorine atom bridges result from edge-sharing, square-based pyramids with a chlorine substituent in the axial position. Interestingly, $[Cl_3(PPh_3)Sb]$ adopts a centrosymmetric dimer, while $[Cl_3(PCy_3)Sb]$ adopts a dimer with C_2 symmetry. The bridging Sb−Cl distances are longer than those involving the terminal chlorine centers.

The bis-phosphine complexes $[Cl_3(PR_3)_2Sb]$ all adopt monomeric structures in the solid state with meridionally configured chlorine substituents. The phosphine ligands are *cis*-configured in [*mer*-Cl_3-*cis*-$(PMe_3)_2Sb$], while a *trans* configuration is observed for [*mer*-Cl_3-*trans*-$(PPh_3)_2Sb$] and [*mer*-Cl_3-*trans*-$(PCy_3)_2Sb$]. We envisage that the sixth coordination site at antimony in these complexes is occupied by a lone pair of electrons. The alternative configuration [*fac*-Cl_3-*cis*-$(PR_3)_2Sb$] is not observed.

The P−Sb and Sb−Cl bond lengths in derivatives of $[Cl_3(PR_3)Sb]$ and $[Cl_3(PR_3)_2Sb]$ are compared graphically in Figure 3, coded according to the substituent (or lone pair) that is *trans* to the P−Sb and Sb−Cl bonds, respectively. Derivatives of $[Cl_3(PR_3)Sb]$ exhibit average P−Sb lengths (horizontal lines in Figure 3 left) that are consistent with the relative Lewis basicity of the phosphine. Longer P−Sb bonds are observed in the analogous derivatives of $[Cl_3(PR_3)_2Sb]$, imposed in the PPh_3 and PCy_3 derivatives by the *trans* configuration and influence of the phosphines. The *cis* configuration of the phosphines observed in [*mer*-Cl_3-*cis*-$(PMe_3)_2Sb$] avoids the *trans* influence of the phosphines with the greatest basicity, resulting in the shortest average P−Sb bonds within the $[Cl_3(PR_3)_2Sb]$ series. The significantly longer bonds in [*mer*-Cl_3-*trans*-$(PCy_3)_2Sb$] is due to a greater basicity and steric presence of PCy_3. The P−Sb or Sb−Cl bonds *trans* to a chlorine atom (2, ○) are observed with intermediate length between those *trans* to a phosphine and those *trans* to a lone pair (Figure 3, ◇). Consequently, *trans* Cl−Sb−Cl arrangements are preferred over *trans* P−Sb−Cl and *trans* P−Sb−P arrangements. The *trans* P−Sb−Cl arrangement is tolerated by the relatively low basicity of PPh_3 in [*fac*-$Cl_3(PPh_3)Sb$] and is

dx.doi.org/10.1021/ic500723y | *Inorg. Chem.* 2014, 53, 5359−5372

Table 2. Selected Structural Parameters for Derivatives of $[Cl_3(PR_3)Sb]$ and $[Cl_3(PR_3)_2Sb]$

	$[Cl_3(PMe_3)Sb]$	$[Cl_3(PPh_3)Sb]$	$[Cl_3(PCy_3)Sb]$	$[Cl_3(PMe_3)_2Sb]$	$[Cl_3(PPh_3)_2Sb]$	$[Cl_3(PCy_3)_2Sb]$
P_A-Sb	2.5951(9) Sb_A	2.7576(5)	2.6516(14)	2.5757(4)	2.7934(4)	2.848(2)
P_B-Sb	2.5962(9) Sb_B			2.7278(4)	2.7934(4)	2.871(2)
P−C	1.791(3)−1.800(3)	1.8047(18)−1.8124(18)	1.828(5)−1.836(5)	1.7953(15)−1.8136(16)	1.8082(17)−1.8144(16)	1.8514(16)−1.8553(17)
$Sb-Cl_A$	2.7656(9) Sb_A-Cl_A 2.8204(9) Sb_B-Cl_A 2.9504(9) $Sb_A-Cl_{A'}$ 2.7083(9) $Sb_B-Cl_{A''}$	2.7562(5) Cl_A 2.8949(5) $Cl_{A'}$	2.3362(14)	2.6046(4)	2.5571(5)	2.568(2)
$Sb-Cl_B$	2.4062(9) Sb_A-Cl_B 2.5093(9) $Sb_B-Cl_{B'}$	2.4037(5)	2.5773(15)	2.5653(4)	2.5572(5)	2.556(2)
$Sb-Cl_C$	2.4783(9) Sb_A-Cl_C 2.4688(9) $Sb_B-Cl_{C'}$	2.3569(5)	2.5939(14) Sb_A-Cl_C 3.269(2) $Sb_A-Cl_{C'}$	2.7096(4)	2.3849(6)	2.3773(12)
P_A-Sb-P_B				93.078(12)	171.862(17)	172.95(4)
$P_A-Sb-Cl_A$	77.55(3) Cl_A 76.68(3) $Cl_{A'}$	170.589(14)	94.96(4)	82.194(12)	85.936(15)	90.60(6)
$P_A-Sb-Cl_B$	90.32(3)	91.732(16)	86.64(5)	86.846(12)	93.727(15)	89.42(6)
$P_A-Sb-Cl_C$	87.67(3)	86.517(16)	86.43(5)	78.331(12)	85.931(9)	86.41(5)
$P_B-Sb-Cl_A$	77.04(3) Cl_A 79.65(3) $Cl_{A''}$			86.805(12)	93.727(15)	89.17(6)
$P_B-Sb-Cl_B$	87.73(3) $Cl_{B'}$			80.240(12)	85.938(15)	89.85(6)
$P_B-Sb-Cl_C$	88.54(3) $Cl_{C'}$			170.333(12)	85.931(9)	86.56(5)
$Cl_A-Sb-Cl_B$	88.91(3) $Cl_A-Sb_A-Cl_B$ 89.62(3) $Cl_A-Sb_B-Cl_{B'}$	94.561(17) Cl_A 176.645(15) $Cl_{A'}$	89.15(5)	162.547(13)	175.27(2)	172.12(4)
$Cl_A-Sb-Cl_C$	165.22(3) $Cl_A-Sb_A-Cl_C$ 165.58(3) $Cl_A-Sb_B-Cl_{C'}$	86.235(17)	87.68(5)	96.297(14)	87.635(11)	84.45(6)
$Cl_B-Sb-Cl_C$	90.77(4) $Cl_B-Sb_A-Cl_C$ 89.85(3) $Cl_{B'}-Sb_B-Cl_{C'}$	92.406(19)	171.90(5)	94.726(14)	87.635(11)	87.68(6)

dx.doi.org/10.1021/ic500723y | Inorg. Chem. 2014, 53, 5359−5372

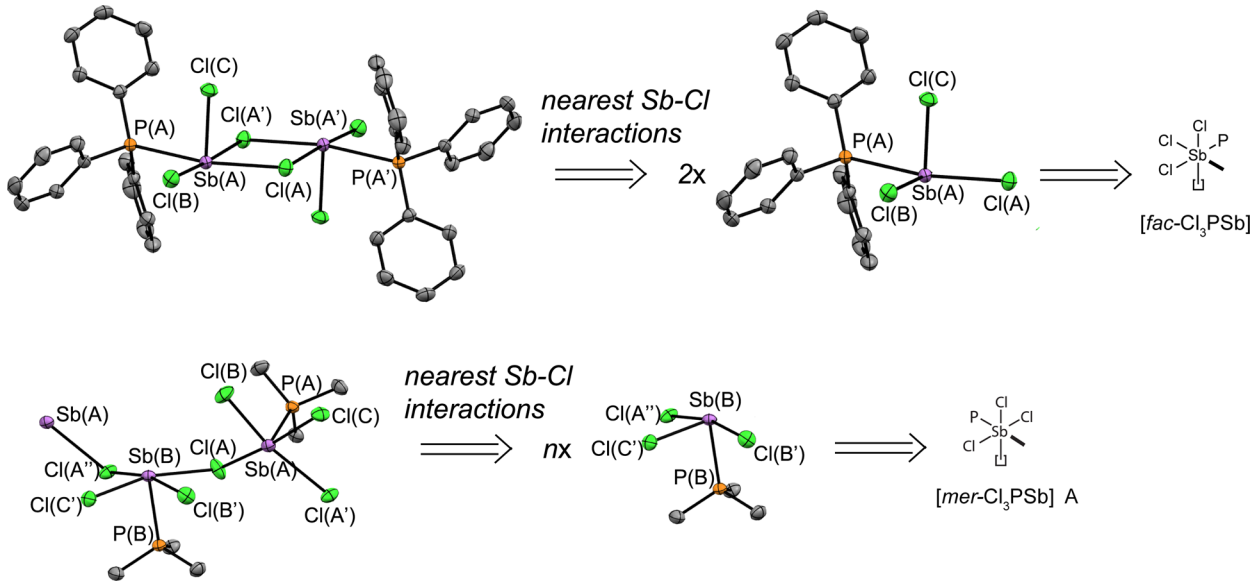

Figure 2. Illustrating the local configuration at antimony for the dimeric [*fac*-$Cl_3(PPh_3)Sb$] (top) and polymeric [*mer*-$Cl_3(PCy_3)Sb$] (bottom).

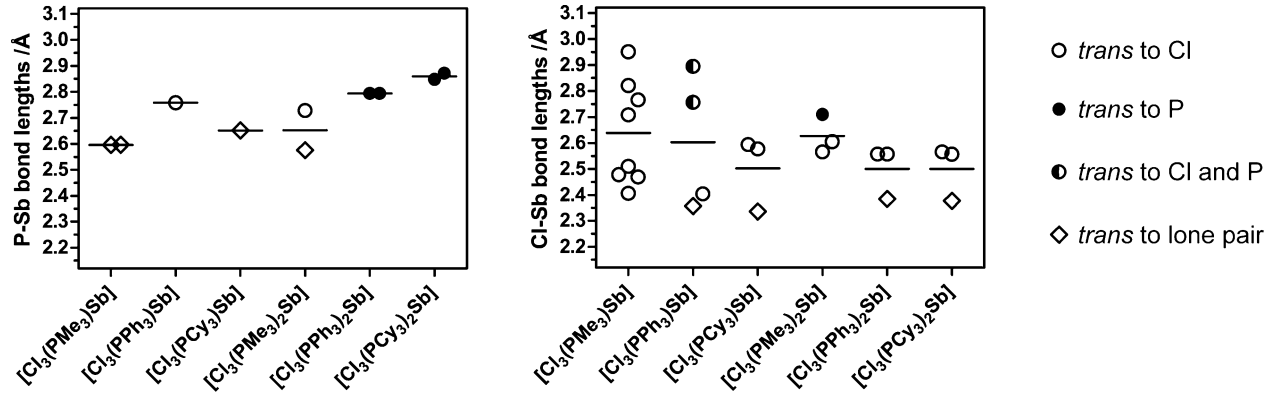

Figure 3. P−Sb (left) and Sb−Cl (right) bond lengths in derivatives of [$Cl_3(PR_3)Sb$] and [$Cl_3(PR_3)_2Sb$], coded according to the substituent *trans* to that bond. Horizontal bars indicate the average value for the compound.

enforced in [*mer*-Cl_3-*cis*-$(PMe_3)_2Sb$] to avoid the *trans* configuration of the more basic PMe_3 ligands. The *trans* P−Sb−P arrangements observed for [*mer*-Cl_3-*trans*-$(PPh_3)_2Sb$] and [*mer*-Cl_3-*trans*-$(PCy_3)_2Sb$] are unavoidable due to the greater steric presence of PPh_3 and PCy_3, compared to PMe_3. On the basis of these structural comparisons, we conclude that in the coordination sphere of antimony in neutral phosphine complexes, the magnitude of *trans* influence has the trend: lone pair < $PPh_3 \leq Cl^- < Cy_3P \approx PMe_3$.

Calculations on gas-phase models using dispersion-corrected DFT (B3LYP-D[12]) were carried out to determine the reaction enthalpies (ΔH_r) and free energies (ΔG_r) for the formation of [$Cl_3(PR_3)Sb$] (R = Me, Ph) according to Scheme 1a, under standard conditions. Geometry optimization revealed the global minimum as a trigonal pyramidal C_{3v} symmetry configuration, [*pyr*-$Cl_3(PR_3)Sb$] **8**, with the phosphine in the apical position and the antimony below the basal plane, consistent with previous theoretical investigations.[31] However, there are no experimental data for such a non-VSEPR geometry, and the observed [*mer*-$Cl_3(PMe_3)Sb$] is a shallow minimum, observed only when using the strictest convergence criterion and when the angle between two chlorine substituents is restricted to greater than 175 degrees. We conclude that the *fac*- and *mer*-configurations observed for [$Cl_3(PR_3)Sb$] result from intermolecular interactions evidenced in the solid state.

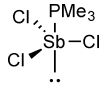

8

The reaction enthalpies (Table 3) for complexes of PMe_3 are negative (exothermic) and small, as expected for closed-shell interactions. However, the entropic costs of complexation are sufficiently high that the overall free-energy changes for the observed *mer* and *fac* isomers are positive (nonspontaneous).

Table 3. Calculated (B3LYP-D with Counterpoise Correction) Enthalpies and Free Energies for Reaction of Cl_3Sb with PR_3 to give [$Cl_3(PR_3)Sb$] in kJ mol^{-1}

	[$Cl_3(PMe_3)Sb$]		[$Cl_3(PPh_3)Sb$]	
	ΔH_r	ΔG_r	ΔH_r	ΔG_r
[*fac*-$Cl_3(PR_3)Sb$]	−18.0	+21.8	+105.9	+151.9
[*mer*-$Cl_3(PR_3)Sb$]	−9.2	+33.1	+140.6	+192.9
[*pyr*-$Cl_3(PR_3)Sb$] **8**	−93.7	−11.8	−49.4	+10.5

dx.doi.org/10.1021/ic500723y | *Inorg. Chem.* 2014, 53, 5359−5372

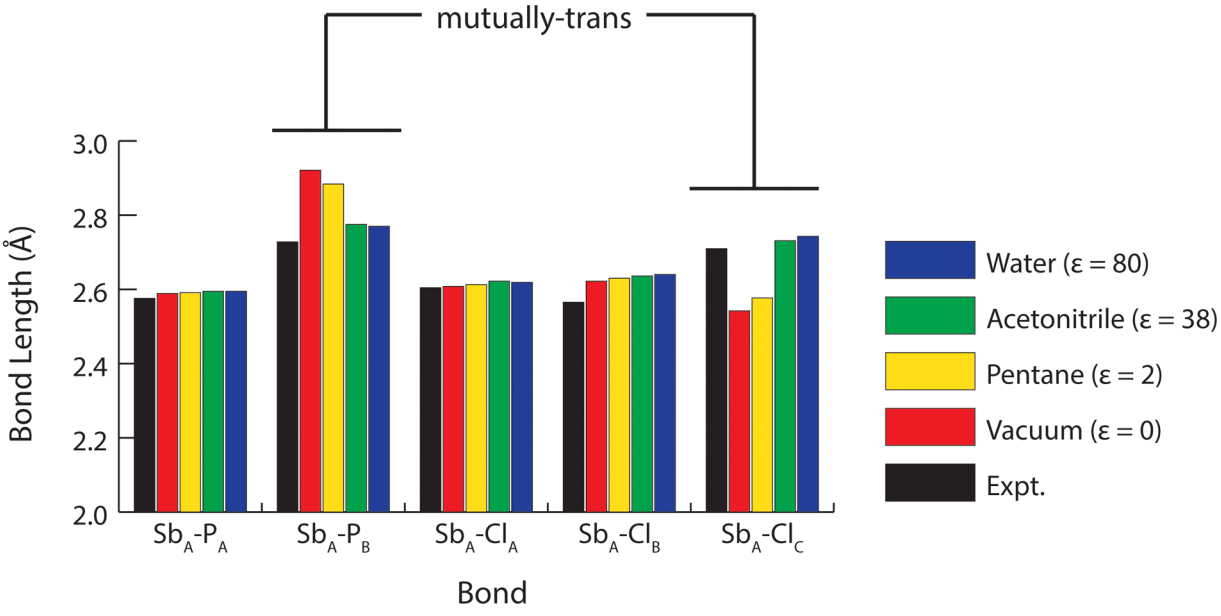

Figure 4. Variations in selected calculated bond lengths for [*mer*-Cl_3-*cis*-$(PMe_3)_2Sb$] as a function of the dielectric constant (ε) of the applied PCM solvent field.

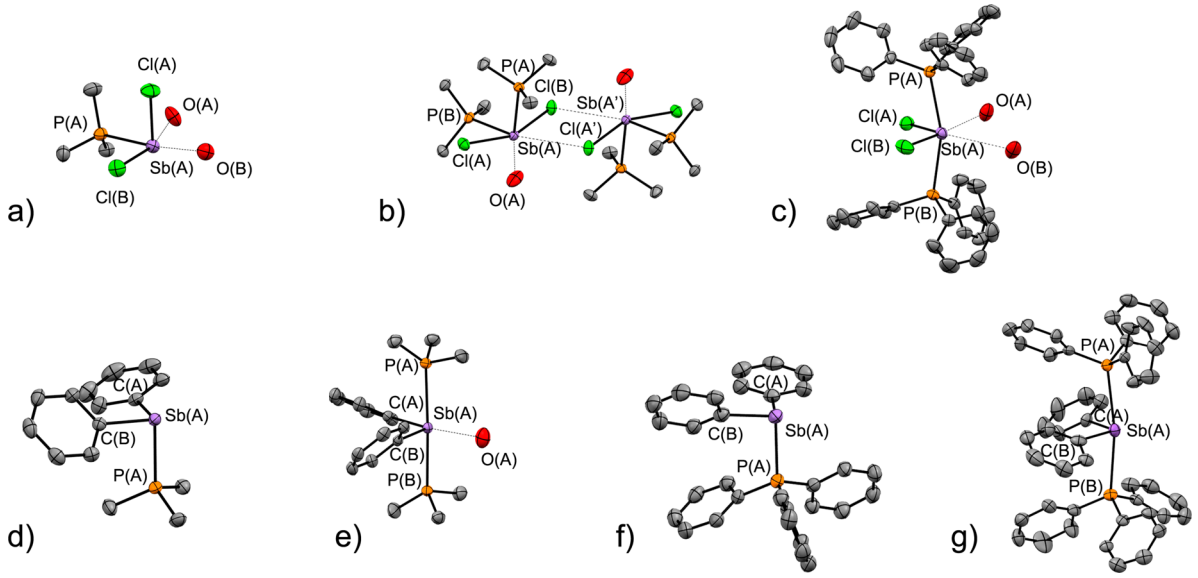

Figure 5. Solid-state structures of the cation in (a) [*fac*-$Cl_2(PMe_3)Sb$][OTf], showing Sb---O contacts, (b) [*trans*-Cl_2–*cis*-$(PMe_3)_2Sb$][OTf], showing the dimeric interactions and Sb---O contacts, (c) [*cis*-Cl_2-*trans*-$(PPh_3)_2Sb$][OTf], showing Sb---O contacts, (d) [*fac*-$Ph_2(PMe_3)Sb$][OTf], (e) [*cis*-Ph_2-*trans*-$(PMe_3)_2Sb$][OTf], showing Sb---O contact, (f) [*fac*-$Ph_2(PPh_3)Sb$][PF_6], and (g) [*cis*-Ph_2-*trans*-$(PPh_3)_2Sb$][PF_6].

The polymeric solid-state structure of [$Cl_3(PMe_3)Sb$] results from intermolecular coordination of a chlorine center from an adjacent [$Cl_3(PMe_3)Sb$] complex. The gas-phase reaction free energies predict that all three configurations of [$Cl_3(PPh_3)Sb$] are unstable with respect to the starting reagents, consistent with the importance of intermolecular lattice interactions in the stability of the complex.

The calculated gas-phase structures for derivatives of [$Cl_3(PR_3)_2Sb$] failed to reproduce the experimental geometric parameters. For instance, the calculated gas-phase (vacuum) structure of [*mer*-Cl_3-*cis*-$(PMe_3)_2Sb$] (Figure 4) shows good agreement with the experimentally observed Sb_A–P_A (Δ = 0.01 Å; Δ = calcd − expt), Sb_A–Cl_A (Δ = 0.01 Å), and Sb_A–Cl_B (Δ = 0.05 Å) distances, but the calculations overestimate the Sb_A–P_B distance by 0.19 Å and underestimate the Sb_A–Cl_C distance by 0.17 Å. In the gas phase, one ligand is bound only weakly, affecting a relatively short Sb_A–Cl_C bond *trans* to the long P_B–Sb_A bond. One calculated imaginary frequency is associated with S_N2-type displacement of Cl_C from the metal center by P_B. Calculations in a simulated solvent field (PCM) of pentane (dielectric constant, ε = 1.84), acetonitrile (ε = 37.5), or water (ε = 80.1) show that greater solvent field polarity recovers the experimentally observed structural parameters (Figure 4). We conclude that calculated gas-phase Sb_A–P_B and Sb_A–Cl_C distances for [*mer*-Cl_3-*cis*-$(PMe_3)_2Sb$] model the initial steps of an SN_2-type nucleophilic displacement of a chloride anion by a phosphine ligand at the antimony center. In solvents of greater polarity, the minimum energy structure is farther along the reaction coordinate toward $[Cl_2(PMe_3)_2Sb]^{1+}$.

dx.doi.org/10.1021/ic500723y | *Inorg. Chem.* 2014, 53, 5359−5372

Table 4. Selected Structural Parameters for [*fac*-$Cl_2(PMe_3)Sb$][OTf], [*trans*-Cl_2-*cis*-$(PMe_3)_2Sb$][OTf], [*cis*-Cl_2-*trans*-$(PPh_3)_2Sb$][OTf], [*fac*-$Ph_2(PMe_3)Sb$][OTf], [*cis*-Ph_2–*trans*-$(PMe_3)_2Sb$][OTf], [*fac*-$Ph_2(PPh_3)Sb$][PF_6], [*cis*-Ph_2-*trans*-$(PPh_3)_2Sb$][PF_6]

	[$Cl_2(PMe_3)Sb$] [OTf]	[$Ph_2(PMe_3)Sb$] [OTf]	[$Ph_2(PPh_3)Sb$] [PF_6]	[$Ph_2(PMe_3)Sb]_4$ [Cl][$PF_6]_3$	[$Ph_2(PMe_3)Sb]_4$ [Br][$PF_6]_3$
P_A–Sb	2.6043(9)	2.5584(4)	2.5950(12)	2.5906(14)	2.5846(13)
P–C	1.797(3)–1.809(3)	1.7981(16)–1.8047(17)	1.794(4)–1.805(5)	1.800(6)–1.804(6)	1.798(5)–1.799(4)
Sb–X_A	2.3719(9)	2.1487(15)	2.152(5)	2.153(4)	2.153(3)
Sb–X_B	2.3926(8)	2.1549(15)	2.153(5)	2.153(4)	2.153(3)
Sb---O_A	2.705(2)	3.5475(16)			
Sb---O_B	2.755(2)	3.6882(14)			
P_A–Sb–X_A	90.71(3)	89.55(4)	93.70(12)	89.08(9)	89.43(8)
P_A–Sb–X_B	90.62(3)	94.74(4)	97.61(12)	89.08(9)	89.43(8)
X_A–Sb–X_B	92.78(3)	96.35(6)	100.14(18)	107.64(19)	107.08(16)
ref	this work	this work	8	7	7

	[$Cl_2(PMe_3)_2Sb$] [OTf]	[$Cl_2(PPh_3)_2Sb$] [OTf]	[$Ph_2(PMe_3)_2Sb$] [OTf]	[$Ph_2(PPh_3)_2Sb$] [PF_6]
P_A–Sb	2.5890(4)	2.8621(5)	2.8034(4)	2.8694(8)
P_B–Sb	2.5805(4)	2.8042(5)	2.7559(4)	2.8426(9)
P–C	1.7914(18)–1.8005(16)	1.810(2)–1.818(2)	1.8047(19)–1.812(2)	1.811(12)–1.833(11)
Sb–X_A	2.6707(4)	2.3643(6)	2.1594(17)	2.157(2)
Sb–X_B	2.5079(4)	2.4083(6)	2.1558(16)	2.157(3)
Sb---O_A	2.996(1)	2.6793(17)	3.4951(19)	
Sb---O_B		3.2332(18)		
P_A–Sb–P_B	101.754(13)	160.901(17)	177.142(13)	170.11(8)
P_A–Sb–X_A	79.283(13)	81.519(18)	86.64(4)	87.9(2)
P_A–Sb–X_B	87.027(14)	84.404(19)	89.60(4)	86.9(3)
P_B–Sb–X_A	79.634(14)	82.142(18)	90.51(4)	86.5(2)
P_B–Sb–X_B	87.122(14)	88.230(19)	90.90(4)	86.2(3)
X_A–Sb–X_B	158.504(14)	98.27(3)	95.06(6)	101.1(3)
ref	this work	this work	this work	8

Structure and Bonding in Cationic Phosphine Complexes of Antimony. The solid-state structures of the cations in [*fac*-$Cl_2(PMe_3)Sb$][OTf], [*trans*-Cl_2-*cis*-$(PMe_3)_2Sb$][OTf], [*cis*-Cl_2-*trans*-$(PPh_3)_2Sb$][OTf], [*fac*-$Ph_2(PMe_3)Sb$][OTf], and [*cis*-Ph_2-*trans*-$(PMe_3)_2Sb$][OTf] are illustrated in Figure 5 and are compared with the structures of the previously reported [*fac*-$Ph_2(PPh_3)Sb$][PF_6] and [*cis*-Ph_2-*trans*-$(PPh_3)_2Sb$][PF_6].[8] Selected structural parameters for these compounds are listed in Table 4. All triflate derivatives in Table 4 are considered to be ionic, exhibiting Sb---O contacts that are substantially greater than the sum of the covalent radii (Σ_{CR} Sb–O = 2.05 Å). The cation in [*fac*-$Cl_2(PMe_3)Sb$][OTf] (Figure 5a) involves two interion Sb---O contacts imposing a square pyramidal geometry at antimony. Similar structures are observed for the cations in [*fac*-$Ph_2(PMe_3)Sb$][OTf] (Figure 5d) and [*fac*-$Ph_2(PMe_3)Sb]_4$[Cl][$PF_6]_3$ (Figure 5f).[7] The bisphosphine cations in [*trans*-Cl_2-*cis*-$(PMe_3)_2Sb$][OTf] (Figure 5b) and [*cis*-Cl_2-*trans*-$(PPh_3)_2Sb$][OTf] (Figure 5c) illustrate further structural variety for antimony. The *cis* configuration of the more basic PMe_3 ligands in the structure of in the cation of [*trans*-Cl_2-*cis*-$(PMe_3)_2Sb$][OTf] is consistent with that of [*mer*-Cl_3-*cis*-$(PMe_3)_2Sb$] and contrasts the *trans* configuration of the phosphines in the cation of [*cis*-Cl_2-*trans*-$(PPh_3)_2Sb$][OTf], made possible by the less basic PPh_3 ligands and the steric stress imposed by phenyl substituents. A *trans* configuration of two PMe_3 ligands is uniquely observed in the cation of [*cis*-Ph_2-*trans*-$(PMe_3)_2Sb$][OTf] (Figure 5e), suggesting that aryl substituents are the most strongly *trans*-labilizing of the groups discussed here, and the trend in the magnitude of *trans* influence: lone pair < PPh_3 ≤ Cl^- < Cy_3P ≈ PMe_3 <Ph^-.

Derivatives of $[Ph_2(PR_3)_2Sb]^{1+}$ (R = Me, Ph) adopt P–Sb distances that are shorter by approximately 0.08 Å when R = Me. The Sb–Cl distances are more sensitive (range of 0.21 Å) to the substitution pattern around Sb. Complexes with shorter P–Sb distances show longer Sb–Cl bond lengths. By comparison, in complexes featuring Ph_2Sb centers, the Sb–C_{phenyl} distances are relatively unperturbed by the variation of the number or type of phosphine ligand (range of 0.01 Å), consistent with the greater elasticity in the more polarized (more ionic) Sb–Cl bond than in the less polarized (more covalent) Sb–C bond.

Structure and Bonding in a Dicationic Phosphine Complex of Antimony. Two views of the dication in the solid-state structure of [*fac*-$Cl(PMe_3)_2Sb$][OTf]$_2$ are shown in Figure 6, one illustrating the three closest contacts to oxygen atoms of anions (a), and the other showing the dimeric association of the formula units through bridging O–S–O units of the anions (b). The definitive facial configuration of the chlorine substituent and two phosphine ligands and the oxygen centers of three separate triflate units impose a distorted octahedral environment for antimony. The Sb---O contacts are comparable in length to the shorter contacts in the monocationic salts (Table 4) and are substantially greater than the sum of the covalent radii (Σ_{CR} Sb–O = 2.07 Å), defining an ionic formulation. The P–Sb bond lengths in the dication are predictably short but are in the range that is observed for neutral and cationic phosphine complexes of antimony. The very short Sb–Cl bond [2.3511(4) Å] is inside the sum of the covalent radii for the two elements (Σ_{CR} Sb–Cl = 2.38 Å).

The *trans* Influence in Phosphine Complexes of Antimony. The trend in the magnitude of *trans* influence at the antimony acceptor site (lone pair < PPh_3 ≤ Cl^- < PCy_3 ≈ PMe_3 <Ph^-) is further demonstrated in the neutral complexes

dx.doi.org/10.1021/ic500723y | Inorg. Chem. 2014, 53, 5359–5372

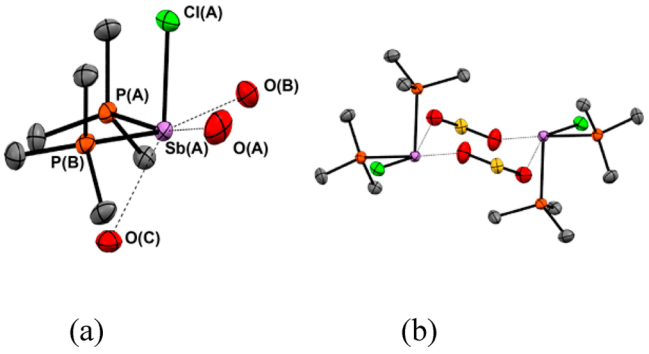

Figure 6. Solid-state structural features in [*fac*-Cl(PMe_3)$_2$Sb][OTf]$_2$, showing (a) the cation with Sb---O contacts and (b) the Sb---OSO---Sb interion contacts between adjacent cations. Thermal ellipsoids are drawn at the 30% probability level. Hydrogen atoms have been omitted for clarity. Select bond lengths (Å) and angles (deg): P_A–Sb_A = 2.5950(4), P_B–Sb_A = 2.5843(4), Sb_A–Cl_A = 2.3511(4), Sb_A–O_A = 2.7922(13), Sb_A–O_B = 2.8459(14), Sb_A–O_C = 2.7114(13), P_A–Sb_A–P_B = 102.026(15), Cl_A–Sb_A–P_A = 90.111(15), Cl_A–Sb_A–P_B = 91.812(15), O_A–Sb_A–O_B = 103.36(5), Cl_A–Sb_A–O_C = 153.19(3).

featuring PR_3, Cl^-, and Ph^- on the same antimony center. The solid-state structures of [Cl_2(Ph)(PMe_3)Sb], [Cl_2(Ph)(PPh_3)Sb], and [Cl_2(Ph)(PPh_3)$_2$Sb] are shown in Figure 7, and selected structural parameters are listed in Table 5. The weakly *trans*-labilizing chlorine substituents in the three compounds allow for the observed *trans* Cl–Sb–Cl configurations in all three structures. Consistently, the more *trans*-labilizing PMe_3 ligand and Ph^- substituent are *cis* configured. In this context, the *trans* labilizing trend defined above enables rationalization and prediction of the configurations even with the variety of VSEPR-consistent configurational options available for derivatives of [Cl_2(Ph)(PR_3)Sb] and [Cl_2(Ph)(PR_3)$_2$Sb] illustrated in Chart 2.

Structure and Bonding in an Anionic Phosphine Complex of Antimony. Hypervalent centers such as those in pnictogen pentafluorides are powerful Lewis acids and react with halides to give weakly coordinating hexahalopnictogen anions. Indeed anionic $[SbCl_4]^{1-}$ is sufficiently Lewis acidic to form the square-based pyramidal (AX_4E) dianion $[SbCl_5]^{2-}$ in the presence of excess chloride anions.[13] The anions $[dmpeSbI_4]^{1-}$ and $[(Et_3P)_2Sb_2Br_7]^{1-}$ have also been reported as serendipitous products of a hydrolysis reaction.[6] In this context, preparation of [$Mg(CH_3CN)_6$][$Cl_4(PMe_3)Sb$]$_2$ from PMe_3 and [$Mg(CH_3CN)_6$][Cl_4Sb]$_2$ represents a rational synthesis of the complex anion. Formation of $[Cl_4(PPh_3)Sb]^{1-}$ is precluded by the relatively low basicity of PPh_3.

The molecular structure of the $[Cl_4(PMe_3)Sb]^{1-}$ anion is derived from $[Cl_5Sb]^{2-}$ by replacing the apical chloride ion with a PMe_3 ligand (Figure 8). The Sb–Cl bonds [2.555(2)–2.634(2) Å, average 2.593 Å] are on average shorter than the basal Sb–Cl bonds in $[Cl_5Sb]^{2-}$ [2.4775(12)–2.8847(12) Å, average 2.646 Å][14] and those in $[Cl_4Sb]^{1-}$ [2.4317(7)–2.6395(11) Å, average 2.536 Å].[15] The magnesium center is not engaged by the phosphine due to encapsulation of the hard $[Mg]^{2+}$ atom with hard CH_3CN ligands (solvent), leaving the soft $[Cl_4Sb]^{1-}$ anion as the sole coordination site for the soft phosphine donor.

Coordination of a Lewis base to cationic or neutral haloantimony centers is understood as donor occupation of vacant p-orbitals or low-lying σ^* Sb–X antibonding orbitals at antimony. As shown in Figure 9, phosphine coordination to anionic $[Cl_4Sb]^{1-}$ also involves overlap of the Me_3P lone pair and a vacant p-orbital perpendicular to the $SbCl_4$ plane (HOMO–1). Bonding within the $SbCl_4$ plane involves overlap between the chlorine lone pairs and the two remaining p-orbitals (HOMO-11, HOMO-12), a small degree of Cl---Cl bonding via in-phase overlap of the chlorine p-orbitals in a ring around Sb (HOMO-9), and delocalized π-bonding involving the chlorine lone-pairs and the p-orbital that is used for P–Sb bonding (HOMO-10). A nonbonding lone pair is evident as the HOMO, thereby accounting for the five bonding pairs and one nonbonding pair of electrons around Sb in six molecular orbitals.

A Charge-Variant Series of PMe_3 Complexes of Chloroantimony Centers. The compounds described above, together with $[(PMe_3)_3Sb]^{3+}$,[11] include the extensive charge-variant series $[Cl_4(PMe_3)Sb]^{1-}$, $[Cl_3(PMe_3)Sb]$, $[Cl_2(PMe_3)Sb]^{1+}$, $[Cl_3(PMe_3)_2Sb]$, $[Cl_2(PMe_3)_2Sb]^{1+}$, $[Cl(PMe_3)_2Sb]^{2+}$, and $[(PMe_3)_3Sb]^{3+}$, for which selected bond lengths are illustrated graphically in Figure 10. Notwithstanding the outlier long P–Sb bond for [$Cl_3(PMe_3)_2Sb$] corresponding to the only P–Sb bond that is *trans* to a chloride substituent, the Sb–Cl bonds adopt a substantially broader range than the P–Sb bonds. A similar effect is evident for phosphine complexes of tin[16] and bismuth halides.[17]

While a greater positive charge is expected to result in stronger and shorter coordinate bonds, the P–Sb bonds are slightly longer for complexes with greater charge. These results are borne out by the calculations (MP2/Def2-TZVPP) of electronic structure for select complexes (see Supporting Information). For example, the calculated gas-phase geometry of [$Cl_3(PMe_3)Sb$] shows a P–Sb bond (2.542 Å) that is slightly shorter than that calculated for $[Cl_2(PMe_3)Sb]^{1+}$ (2.561 Å). The corresponding Sb–Cl distances for the netural (2.491 Å)

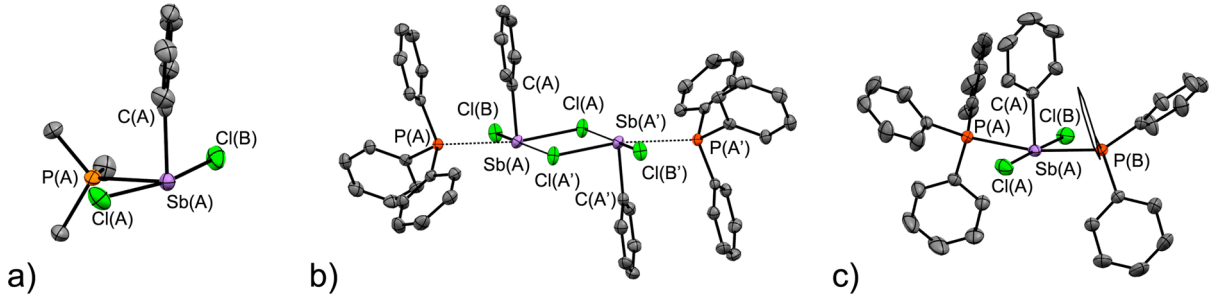

Figure 7. Solid state structures of (a) [Cl_2(Ph)(PMe_3)Sb], II (b) [Cl_2(Ph)(PPh_3)Sb], III and (c) [Cl_2(Ph)(PPh_3)$_2$Sb], VI. The Roman numerals refer to labels in Chart 2.

dx.doi.org/10.1021/ic500723y | *Inorg. Chem.* 2014, 53, 5359–5372

Table 5. Selected Structural Parameters for $[Cl_2(Ph)(PMe_3)Sb]$, $[Cl_2(Ph)(PPh_3)Sb]$, and $[Cl_2(Ph)(PPh_3)_2Sb]$

	$[Cl_2(Ph)(PMe_3)Sb]$	$[Cl_2(Ph)(PPh_3)Sb]$	$[Cl_2(Ph)(PPh_3)_2Sb]$
P_A–Sb	2.5612(4)	2.9656(5)	2.8741(4)
P_B–Sb			2.8741(4)
P–C	1.7971(17)–1.7992(19)	1.819(2)–1.822(2)	1.8174(15)–1.8204(15)
Sb–Cl_A	2.6286(5)	2.3965(6)	2.5989(4)
		Sb_A–Cl_A	
		3.3152(6)	
		Sb_A–$Cl_{A'}$	
Sb–Cl_B	2.5566(5)	2.5463(6)	2.5989(4)
Sb–C_A	2.1640(16)	2.146(2)	2.163(2)
P_A–Sb–P_B			169.098(16)
P_A–Sb–Cl_A	78.952(15)	169.437(19)	85.722(15)
		P_A–Sb_A–$Cl_{A'}$	
		100.920(15)	
		P_A–Sb_A–$Cl_{A'}$	
P_A–Sb–Cl_B	87.297(15)	83.233(18)	94.419(15)
P_A–Sb–C_A	95.85(4)	84.04(6)	84.549(8)
P_B–Sb–Cl_A			94.418(15)
P_B–Sb–Cl_B			85.721(15)
P_B–Sb–C_A			84.548(8)
Cl_A–Sb–Cl_B	165.789(16)	90.09(2)	178.53(2)

Chart 2. VSEPR-Consistent Configurational Options for $[Cl_2(Ph)(PR_3)Sb]$ and $[Cl_2(Ph)(PR_3)_2Sb]$[a]

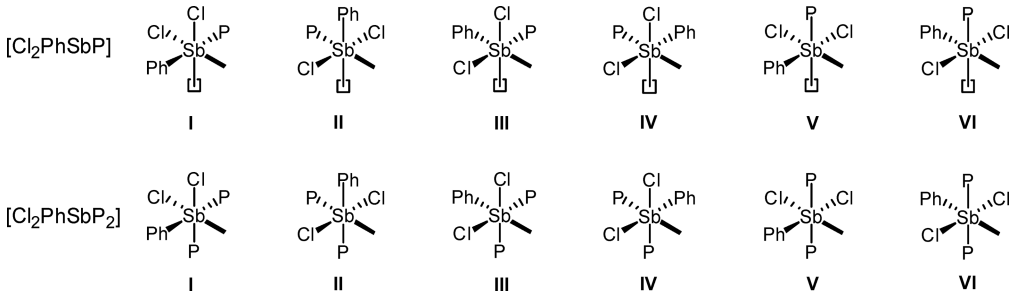

[a]P = phosphine; bold line = lone pair; □ = vacant coordination site.

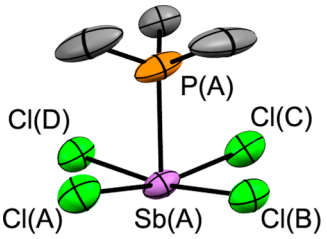

Figure 8. Molecular structure of the anion in $[Mg(CH_3CN)_6][Cl_4(PMe_3)Sb]_2$. One of two asymmetric units is shown. Thermal ellipsoids are drawn at 30% probability level. Hydrogen atoms have been omitted for clarity. Select bond lengths (Å) and angles (deg): P_A–Sb_A = 2.582(2), Sb_A–Cl_A = 2.580(2), Sb_A–Cl_B = 2.634(2), Sb_A–Cl_C = 2.601(2), Sb_A–Cl_D = 2.555(2), P_A–Sb_A–Cl_A = 82.10(7), P_A–Sb_A–Cl_B = 85.53(8), P_A–Sb_A–Cl_C = 88.89(7), P_A–Sb_A–Cl_D = 81.05(8), Cl_A–Sb_A–Cl_B = 90.93(8), Cl_A–Sb_A–Cl_C = 170.93(7), Cl_A–Sb_A–Cl_D = 90.91(7), Cl_B–Sb_A–Cl_C = 89.45(8), Cl_B–Sb_A–Cl_D = 166.08(7), Cl_C–Sb_A–Cl_D = 86.58(7).

and cationic (2.315 Å) complexes show the opposite trend. Similarly, the P–Sb distance in the calculated structure of $[Cl_2(PMe_3)_2Sb]^{1+}$ (2.555 Å) is shorter than in $[Cl(PMe_3)_2Sb]^{2+}$ (2.561 Å), whereas the Sb–Cl distance is shorter for the greater charge (2.507 and 2.317 Å, respectively). These observations are consistent with strengthening of the Sb–Cl bond with increasing charge, predicted by increased electrostatic attraction across the polar Sb–Cl bond. In addition, electronic structure calculations on the model complex $[Cl_2(PMe_3)Sb]^{1+}$ also show (Figure 11) increased Sb–Cl covalency via two π-type bonding MOs (HOMO-4, HOMO-5) delocalized over the Cl–Sb–Cl fragment, evidencing a competitive occupation of a p-orbital at Sb by the phosphine and chlorine lone pairs. This π-type interaction is in addition to two Sb–Cl σ-bonding MOs (HOMO-6, HOMO-8) and may explain preferential shortening of the Sb–Cl bonds at the cost of elongated P–Sb bonds.

The sum of bond angles around the trigonal pyramidal Sb centers in $[Cl_2(PMe_3)Sb]^{1+}$ (274.1°), $[Cl(PMe_3)_2Sb]^{2+}$ (283.9°), and $[(PMe_3)_3Sb]^{3+}$ (305.8°) increase drastically with steric bulk upon stepwise substitution of chlorides with phosphines. For comparison, the sum of the Cl–Sb–Cl bond angle in solid and gaseous $SbCl_3$ is 285.6° and 291.57°, respectively.[18,19] As expected, the extent of pyramidalization around phosphorus decreases only slightly upon successive removal of chlorides in $[Cl_4(PMe_3)Sb]^{1-}$ (319.1°), $[Cl_3(PMe_3)Sb]$ (320.5°), and $[Cl_2(PMe_3)Sb]^{1+}$ (322.2°).

The ^{31}P NMR spectra of derivatives of $[Cl_n(PMe_3)_mSb]^{(3-n)+}$ (n = 1–4, m = 1, 2) in CD_3CN at 298 K are plotted in Figure 12 as a function of the formal charge on the stibine complex. The phosphorus centers in $[Cl_2(PMe_3)_2Sb]^{1+}$ and [Cl-

dx.doi.org/10.1021/ic500723y | Inorg. Chem. 2014, 53, 5359–5372

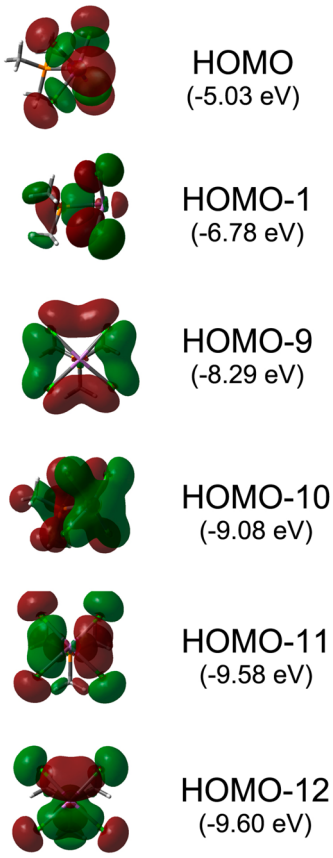

Figure 9. Molecular orbitals (MP2/Def2-TZVPP) relevant to the bonding in $[Cl_4(PMe_3)Sb]^{1-}$. Hydrogen atoms have been omitted for clarity.

$(PMe_3)_2Sb]^{2+}$ are isochronous by symmetry and give rise to a single chemical shift value. For [*mer*-Cl_3-*cis*-$(PMe_3)_2Sb$], only one signal is observed, despite the nonequivalence of the phosphorus centers in its solid-state structure, indicating a dynamic process that exchanges the two phosphines. However, in a low-temperature NMR experiment, the slow-exchange limit characterized by decoalescence and peak separation was not reached at −90 °C, preventing a determination of the chemical shifts for the two environments.

The ^{31}P NMR results are consistent with greater deshielding of the phosphorus nucleus for complexes of higher positive charge. The monophosphine complexes show chemical shifts that are further downfield than their bisphosphine analogues, indicating a distribution of the charge over two phosphines. The effect is most pronounced in complexes of $[Ph_2Sb]^{1+}$, which show ^{31}P chemical shifts of −21.2 ppm and −41.3 ppm for the mono-PMe_3 and bis-PMe_3 complexes, respectively. Similarly, the shift for $[Cl_3(PCy_3)Sb]$ (+25.1 ppm) is 10 ppm downfield of $[Cl_3(PCy_3)_2Sb]$ (+15.7 ppm). By comparison, the ^{31}P chemical shifts of PPh_3 complexes are essentially independent of charge or geometry and are almost identical to that of free PPh_3 (−5.6 ppm). We conclude that even in weakly polar solvents (e.g., CD_2Cl_2), solutions of the PPh_3 complexes consist of dissociated phosphine ligands and solvated $SbCl_3$, $Cl_2Sb(OTf)$, or $Ph_2Sb(OTf)$. The solvation enthalpies of these individual species are therefore approximately equal to the strength of the phosphine-stibine interaction, and in the absence of solvent, crystalline products with P−Sb bonds are obtained in the solid state. Consistently, all observed PPh_3 complexes are soluble in CH_2Cl_2.

CONCLUSIONS

A series of cationic, neutral, and anionic prototypical phosphine complexes of antimony(III) have been prepared and structurally characterized. On the basis of the observed configurations of substituents and ligands at antimony in this series, the relative *trans*-labilizing influence exerted by a lone pair, a substituent or a ligand is concluded to be lone pair < PPh_3 ≤ Cl^- < PCy_3 ≈ PMe_3 < Ar^-. Consistent with this model, all previously reported adducts of $SbCl_3$ with Lewis bases weaker than PMe_3 adopt a facial configuration of chloride substituents,[20,21] while complexes with the strong donors 2,2-bipyridine, 1,3-dimethyl-2-imidazolethione,[22] tetramethylthiourea,[23] or PCy_3 show the meridional configuration of chloride substituents, and the distinction is also evident in the solid-state

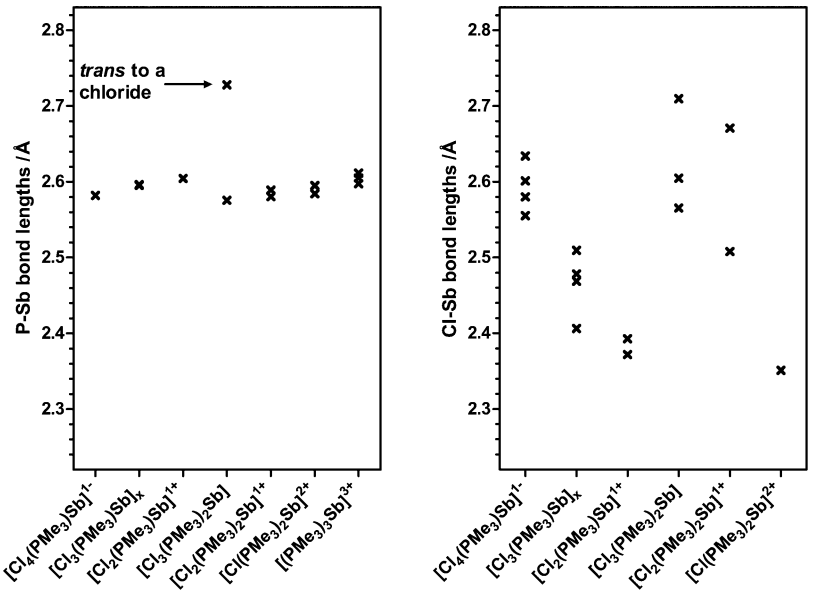

Figure 10. P−Sb (left) and Sb−Cl (right) bond lengths in PMe_3 complexes of chloroantimony acceptors.

dx.doi.org/10.1021/ic500723y | *Inorg. Chem.* 2014, 53, 5359−5372

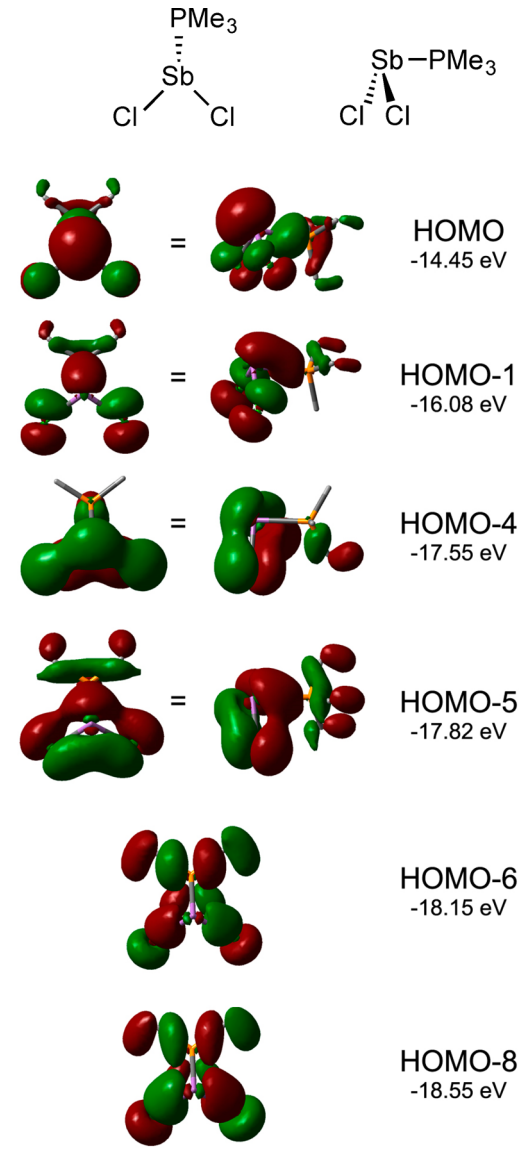

Figure 11. Molecular orbitals (MP2/Def2-TZVPP) relevant to the bonding in $[Cl_2(PMe_3)Sb]^{1+}$. Hydrogen atoms have been omitted for clarity.

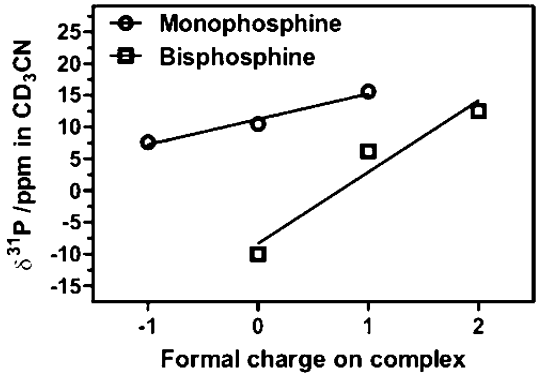

Figure 12. $^{31}P\{^1H\}$ NMR chemical shifts in CD_3CN for observed complexes in the series $[Cl_n(PMe_3)_mSb]^{(3-n)+}$; n = 1−4, m = 1, 2 plotted as a function of the formal charge of the complex.

structures of other antimony halides.[3,24] We expect that the relative *trans*-labilizing influence of these fragments will be broadly applicable to analogous complexes of other main-group acceptor centers bearing a lone pair. We further predict that carbene complexes of the type $[Cl_3(NHC)Sb]$ (NHC = N-heterocyclic carbene) will feature a [*mer*-$Cl_3(NHC)Sb$] A configuration, since carbenes are stronger donors than the most basic phosphines. By corollary, donors weaker than phosphines, such as dialkylsulfides, will adopt a [*fac*-Cl_3LSb] configuration.

Calculations on molecules in the gas phase suggest that the 1:1 neutral complexes are stable, but the 1:2 stibine/phosphine complexes are unstable with respect to dissociation of one of the phosphine ligands. Nevertheless, they are observed in the solution and solid state due to additional stabilization from intermolecular interactions. We therefore urge caution when interpreting statements regarding the stability of such weakly bound complexes in cases when such conclusions are drawn exclusively from gas-phase modeling. Comparison of the experimental structural data for a charge-variant series of PMe_3 complexes of haloantimony centers reveals counter-intuitive differences in the P−Sb and Sb−Cl bond lengths, which are explained with reference to increased ionic and covalent Sb−Cl bonding, as borne out in computational models. For PMe_3 complexes, solution-phase ^{31}P NMR spectroscopy is a sensitive probe of the overall charge on the complex, while PPh_3 complexes dissociate in solution and show only the free ligand.

There is renewed interest in the development of ligand-stabilized main-group halides, with a view toward using their reduction chemistry to access species featuring multiply-bonded elements. While most efforts have been directed toward carbene-stabilized main-group centers,[25−28] we have successfully demonstrated analogous reductive coupling chemistry for phosphine-stabilized cationic halophosphine[29,30] and halostibine[11,31] centers. Moreover, a recent theoretical investigation has made specific predictions about the viability of accessing phosphine-stabilized group 15 element dimers (E-E triple-bonded molecules) from phosphine-ECl_3 adducts.[32] The complexes presented here represent ideal precursors to test these predictions.

■ ASSOCIATED CONTENT

Supporting Information

IR/Raman characterization of selected compounds; Cartesian coordinates for calculated structures; crystallographic information files. This material is available free of charge via the Internet at http://pubs.acs.org.

■ AUTHOR INFORMATION

Corresponding Author

*Fax: +1 250 721 7147; tel: +1 250 721 7150; e-mail: nburford@uvic.ca.

Notes

The authors declare no competing financial interest.

■ REFERENCES

(1) Burford, N.; Ragogna, P. J. *J. Chem. Soc., Dalton Trans.* **2002**, 4307−4315.

(2) Petuškova, J.; Bruns, H.; Alcarazo, M. *Angew. Chem., Int. Ed.* **2011**, *50* (16), 3799−3802. Petuškova, J.; Patil, M.; Holle, S.; Lehmann, C. W.; Thiel, W.; Alcarazo, M. *J. Am. Chem. Soc.* **2011**, *133*, 20758−20760. Carreras, J.; Patil, M.; Thiel, W.; Alcarazo, M. *J. Am. Chem. Soc.* **2012**, *134*, 16753−16758.

(3) Clegg, W.; Elsegood, M. R. J.; Graham, V.; Norman, N. C.; Pickett, N. L.; Tavakkoli, K. *J. Chem. Soc., Dalton Trans.* **1994**, 1743−1751.
(4) Genge, A. R. J.; Hill, N. J.; Levason, W.; Reid, G. *J. Chem. Soc., Dalton Trans.* **2001**, 1007−1012.
(5) Burford, N.; M. D'eon, P. J.; Ragogna, R.; McDonald; Ferguson, M. J. *Inorg. Chem.* **2004**, *43* (2), 734−738.
(6) Clegg, W.; Elsegood, M. R. J.; Graham, V.; Norman, N. C.; Pickett, N. L. *J. Chem. Soc., Dalton Trans.* **1994**, 1753−1757.
(7) Wielandt, J. W.; Kilah, N. L.; Willis, A. C.; Wild, S. B. *Chem. Commun.* **2006**, 3679−3680.
(8) Kilah, N. L.; Petrie, S.; Stranger, R.; Wolfram Wielandt, J.; Willis, A. C.; Wild, S. B. *Organometallics* **2007**, *26* (25), 6106−6113.
(9) Price, J. T.; Lui, M.; Jones, N. D.; Ragogna, P. J. *Inorg. Chem.* **2011**, *50*, 12810−12817.
(10) Chitnis, S. S.; Peters, B.; Conrad, E.; Burford, N.; McDonald, R.; Ferguson, M. J. *Chem. Commun.* **2011**, *47*, 12331−12333.
(11) Chitnis, S. S.; Carpenter, Y.-Y.; Burford, N.; McDonald, R.; Ferguson, M. J. *Angew. Chem., Int. Ed.* **2013**, *52*, 4863−4866.
(12) The B3LYP functional was used with Grimme's empirical dispersion correction (S_6 = 1.05) included by locally modifying Gaussian 09 via the IOP(3/124=3). Basis set constructions: Def2-TZVPP for P, Sb, Cl atoms; 6-311g(d) for C, H atoms.
(13) Liu, M. *Acta Cryst. Struct. Rep. E* **2011**, *E67*, m1812.
(14) Feng, W.; Shu, Z.; Ma, X.; Jin, Z. *Acta Cryst. Struct. Rep. E* **2007**, *E63*, m2411.
(15) Ghoulili, A.; Chaari, N.; Zouari, F. *X-ray Struct. Anal. Online* **2010**, *26*, 21−26.
(16) MacDonald, E.; Doyle, L.; Chitnis, S. S.; Werner-Zwanziger, U.; Burford, N.; Decken, A. *Chem. Commun.* **2012**, *48*, 7922−7924.
(17) Chitnis, S. S.; Burford, N.; Decken, A.; Ferguson, M. J. *Inorg. Chem.* **2013**, *52* (12), 7242−7248.
(18) Lindqvist, I.; Niggli, A. *J. Inorg. Nucl. Chem.* **1956**, *2*, 345−347.
(19) Cazzoli, G.; Caminato, W. *J. Mol. Spectrosc.* **1976**, *62*, 1−7.
(20) Golic, L.; Miliceu, S. *Acta Crystallogr., Sect. B* **1978**, *34*, 3379−3381. The lower basicity of Ph_3PO relative to Me_3P was confirmed experimentally by quantitative displacement of the phosphine oxide by Me_3P upon addition of the latter to a solution of $[(Ph_3PO)_2SbCl_3]$.
(21) Okuda, T.; Gima, S.; Ishihara, H.; Negita, H. *J. Mol. Struct.* **1982**, 261−268.
(22) Rubin, B.; Heldrich, F. J.; Dean, W. K.; Williams, D. J.; Viehbeck, A. *Inorg. Chem.* **1981**, *20*, 4434−4437.
(23) Hough, E.; Nicolson, D. G. *J. Chem. Soc., Dalton Trans.* **1981**, 2083−2087.
(24) Pohl, S.; Saak, W.; Lotz, R.; Haase, D. *Z. Naturforsch., B* **1990**, *45*, 1355.
(25) Abraham, M. Y.; Wang, Y.; Xie, Y.; Wei, P.; Schaefer, H. F.; Schleyer, P. v. R., III; Robinson, G. H. *Chem.—Eur. J.* **2010**, *16*, 432−435.
(26) Sidiropoulos, A.; Jones, C.; Stasch, A.; Klein, S.; Frenking, G. *Angew. Chem., Int. Ed.* **2009**, *48* (51), 9701−9704.
(27) Wang, Y.; Xie, Y.; Wei, P.; King, R. B.; Schaefer, H. F.; Schleyer, P. v. R., III; Robinson, G. H. *Science* **2008**, *321*, 1069−1071.
(28) Wang, Y.; Xie, Y.; Wei, P.; King, R. B.; Schaefer, H. F.; Schleyer, P. v. R., III; Robinson, G. H. *J. Am. Chem. Soc.* **2008**, *130*, 14970−14971.
(29) Carpenter, Y.; D yker, C. A.; Burford, N.; Lumsden, M. D.; Decken, A. *J. Am. Chem. Soc.* **2008**, *130* (46), 15732−15741.
(30) Dyker, C. A.; Burford, N.; Lumsden, M. D.; Decken, A. *J. Am. Chem. Soc.* **2006**, *128* (30), 9632−9633.
(31) Conrad, E.; Burford, N.; Werner-Zwanziger, U.; McDonald, R.; Ferguson, M. J. *Chem. Commun.* **2010**, *46*, 2465−2467.
(32) Wilson, D. J.; Couchman, S. A.; Dutton, J. L. *Inorg. Chem.* **2012**, *51*, 7657−7668.